Cerium L_{III}-edge EXAFS Investigation of the Structure of Crystalline and Amorphous Cerium Oxides

Ahmed M. Shahin[1] and Thomas P. Schuman[1], Fernande Grandjean[1,2], and Gary J. Long[1]

1-Department of Chemistry, University of Missouri-Rolla, Rolla-MO 65409-0010, USA.
2-Department of Physics, B5, University of Liège, B-4000 Sart, Belgium

Introduction

As a consequence of changing properties, e.g., mechanical, magnetic, or electrical, the nanocrystalline phase of rare earth metal oxides has become of immense interest.[1] Of these, cerium oxides have attracted considerable research interest due to a diversity of applications. For instance, the basicity function of cerium oxide when combined with the hydrogenation property of a metal such as Pt or Pd denotes cerium oxide as a promising conversion catalyst. Thus, cerium oxide can lead to selective hydrogenation catalysis of unsaturated compounds.[2] Of interest is the ability of the cerium oxide to store oxygen. The phenomenon is associated with a fast valence change in the solid, i.e., $Ce^{IV} \leftrightarrow Ce^{III}$, and also with anionic vacancies $CeO_2 \rightarrow CeO_{2-x} + (x/2)O_2$.[3] In this study, we report the synthesis of cerium oxide using different precipitation conditions. We also investigated the valence state of cerium ions and covalence with oxide ligands by varying the reaction conditions.

Experimental section

A dilute aqueous ammonia solution (0.01M) was added dropwise to a mixture of 0.05 mol of an aqueous solution of cerium nitrate hexahydrate, $Ce(NO_3)_3 \cdot 6H_2O$, and hydrogen peroxide. Because the oxidation with H_2O_2 is slow in an acidic media, a few drops (10-20) of aqueous ammonia were added to accelerate the oxidation of Ce^{III} to Ce^{IV}. Cerium oxide was precipitated at two different hydrogen peroxide concentrations. The molar ratios of cerium to hydrogen peroxide were 1:0.8 (sample **I**) and 1:1.2 (sample **II**).

X-Ray Absorption Measurements. X-ray absorption measurements were carried out at the unfocused 4-3 beamline of Stanford Synchrotron Radiation Laboratory. The measurements were carried out in both transmission and fluorescence modes at room temperature.

Results and Discussion

XANES Spectral Results. X-ray diffraction (XRD) patterns of both hydrous CeO_2 and **I** revealed a fluorite structure with a particle size of ~6 nm derived from the line broadening.[4] The particle size of anhydrous CeO_2 was larger than that of hydrous CeO_2 and sample **I**, whereas **II** was amorphous.[4] The XANES spectra for anhydrous CeO_2, hydrous CeO_2, **I**, and **II** are depicted in Figure 1. Four peaks were fit in the XANES spectra, a high energy peak A, main peak B, low energy peak C, and pre-edge peak D. Peaks A and B were assigned as due to a mixture of the multielectron configurations $L4f^{0}5d^{1}$ and $L4f^{1}5d^{1}$, respectively, where L denotes the hole in the $2p$ shell, and $5d^1$ refers to the excited electron in the previously unoccupied $5d$ state.[5] Integration of peak C at ~5723 eV displayed a different area for each of the samples. Based on this and other[4] observations, the electronic transition that occurred at ~5723 eV was interpreted as arising from a combination of crystal field splitting and excitation of different amounts of a Ce^{III} contaminant present in all the samples. Unfortunately, the characteristic white line of a typical Ce^{III} compound, $Ce(NO_3)_3 \cdot 6H_2O$, is observed at the same energy as peak C.[6] No significant change in the white line areas, as determined from the many-body configuration theory for a core transition to localized electronic states, was observed in all of the samples under study. Furthermore, changing the hydrogen peroxide concentration during the precipitation of cerium oxide did not result in a significant change in the electronic cerium mixed-valence state.

Modeling of the XANES spectra, in terms of the one-electron band structure of the crystal for a core transition to delocalized electronic states, is a useful approach to determine the cerium valence state and to support the results obtained from the many-body configuration theory for a core transition to localized electronic states. The XANES features have been calculated using FEFF8.20 code, figure 2.[7] The calculated valences obtained from the XANES spectra simulation using FEFF8.20 are in agreement with those obtained from the many-body configuration theory, Table 1.

EXAFS Spectral Results and Discussion. Results of the fitting of the EXAFS spectra are summarized in Table 2. The extracted k^3-weighted EXAFS oscillations, the corresponding Fourier filtered data, and modeled EXAFS results for anhydrous CeO_2, hydrous CeO_2, **I**, and **II** are shown in Figure 3. The EXAFS spectrum of the amorphous precipitate (sample **II**) exhibited a different structure than that of either anhydrous CeO_2, hydrous CeO_2, or **I**. Above the spurious low-R feature, the major oxygen Fourier transformed peak appeared dampened and had practically non-existent outer-shell, Ce-Ce or Ce-O2, features. The increase of Ce-O1 distance in **II** reflects a high-σ^2 value and the necessity of allowing an additional anharmonic correction term for the O1 path. Visual inspection of the hydrous CeO_2 and **I** spectra showed that the samples' near-neighbor structure deviated significantly from either anhydrous CeO_2 or **II**. The Ce-O1, the Ce-Ce, and the Ce-O2 neighbor coordinations in hydrous CeO_2 appeared more ordered with smaller σ^2 as compared with **I**, or **II**, but less ordered than the crystalline anhydrous CeO_2. Analysis of EXAFS spectrum of **I** indicated comparable oscillation amplitudes to those of hydrous CeO_2. The distance between cerium centers and oxygen neighbors in the first coordination shell are of similar magnitude, 2.360 and 2.364 Å for hydrous CeO_2 and **I**, respectively. However, larger deviations were observed in Ce-Ce and Ce-O2 distances between hydrous CeO_2 and **I** samples. Hydrogen peroxide thus induced changes in the coordination spheres around cerium, longer bond distances and fewer coordinated atoms. The parameters in the EXAFS analysis yielded higher N_{O1} values, higher σ^2, and longer Ce-O bond distances for both hydrous CeO_2, **I**, and especially **II** compared to anhydrous CeO_2. Increasing the coordination number, N1, was attributed to incorporating H_2O molecules that resulted in decreasing the crystalline order. The evaluation of each parameter in going from anhydrous CeO_2 to **II** indicates a decrease in crystalline order. The Fourier transformed peak representing the Ce-Ce interaction of hydrous and **I** were more pronounced than in amorphous **II**, and less pronounced than in crystalline anhydrous CeO_2. The enhanced Ce-Ce distance, and the decreased coordination number, N2, in both hydrous CeO_2 and **I** compared with anhydrous CeO_2 were attributed to a higher degree of defect sites in these nanocrystalline materials.

Conclusions

Different hydrogen peroxide concentrations were employed during the precipitations of cerium oxide. XANES analysis clearly showed a significant change in the intensity of the white line peaks of precipitated cerium oxide revealing a smaller particle size as compared to anhydrous CeO_2. However, no significant change in cerium spectroscopic valence for precipitated cerium oxides was observed, regardless of peroxide concentration, in comparison to the anhydrous CeO_2. Precipitation of cerium oxide utilizing H_2O_2 resulted in an increased bond distance, $R_{Ce\text{-}O}$, as well as coordination number of the first coordination shell Ce-O. A decrease in the coordination numbers of the second shell, Ce-Ce, and the third shell, Ce-O, were observed from the radial distribution function. Furthermore, the Debye-Waller factor for the three shells exhibited a

consistent trend as the value of the three coordination shells increased going from anhydrous CeO_2, hydrous CeO_2, sample **I**, to sample **II**. Based on these observations, the degree of disorder increased with increasing H2O2 concentration during precipitation of cerium oxide, consequently increasing the potential for cerium oxide precipitate to function as oxygen traps. Decreasing the particle size of cerium oxide precipitates, with probable increase in oxygen trapping capability offers additional insight into the enhancement of the fuel cells performance using cerium oxide precipitates.

Table 1. Cerium L_{III}-edge XANES Fits of the Two Characteristic Peaks.

Sample	Anhydrous CeO2	Hydrous CeO2	**I**	**II**
Peak (A) position	5735.1	5735.2	5734.3	5734.7
Peak (A) width	3.5	3.2	3.6	3.8
Peak (B) position	5727.6	5727.1	5726.5	5726.5
Peak (B) width	2.8	2.9	3.0	3.2
Valence-Least square fitting	3.45	3.51	3.47	3.48
FEFF-calculated valence	3.48	3.49	3.51	3.52

Table 2. Parameters Extracted from Least-Squares Fitting of the EXAFS Spectra

Sample	Crystallo-graphic data	Anhydrous CeO2	Hydrous CeO2	**I**	**II**
Ce-O1 R(Å)	2.343	2.343*	2.360 (2)	2.364 (3)	2.420 (1)
Ce-O1 N1	8	8*	9.5 (1)	10 (1.5)	11.5(1.3)
Ce-O1 σ^2 (10^{-3} Å^2)	-	3.20(4)	6.45(5)	9.43(2)	10.22 (6)
Ce-Ce R(Å)	3.826	3.826*	3.847 (3)	4.122 (2)	3.814 (4)
Ce-Ce N1	12	12*	7.4 (1.1)	6.6 (1.6)	3.6 (1)
Ce-Ce σ^2 (10^{-3} Å^2)	-	1.50(2)	3.30(6)	4.20(1)	9.60(2)
Ce-O2 R(Å	4.487	4.487*	4.210 (5)	4.127 (17)	-
Ce-O2 N1	24	24*	18.0 (1.6)	16.1 (1)	-
Ce-O2 σ^2 (10^{-3} Å^2)	-	2.40(1)	3.20(5)	4.80(5)	-

* Fixed parameters

Acknowledgement. Support for this project was provided through the Air Force Research Laboratory Materials and Manufacturing Directorate, project manager Steve Szaruga. Portions of this research were carried out at the Stanford Synchrotron Radiation Laboratory, a national user facility operated by Stanford University on behalf of the U.S. Department of Energy, Office of Basic Energy Sciences.

References

(1) Winterer, M.; Nitsche, R.; Hahn, H., *J. Phys. IV France* **1997**, 7, C2-1211.
(2) Fierro, J. L. G.; Soria, J.; Sanz, J.; Rojo, M. J., *J. Solid State Chem.* **1987**, 66, 154.
(3) Sun, Y.; Sermon, P. A., *J. Mater. Chem.* **1996**, 6, 1025.
(4) Schuman, T., "Cerium oxide pigments for anti-corrosion primer coatings," submitted.
(5) Bianconi, A.; Marcelli, A.; Dexpert, H.; Karnatak, R.; Kotani, A.; Jo, T.; Petiau, J., *Phys. Rev. B* **1987**, 35, 806.
(6) Wu, Z.; Benfield, R. E.; Guo, L.; Li, H.; Yang, q.; Grandjean, D.; Li, q.; Zhu, H., *J. Phys.: Condens. Matter* **1994**, 6, 8429.
(7) Ankudinov , A. L; Bouldin, C.; Rehr, J. J.; Sims, J.; Hung, H., *Phys. Rev. B* **2002**, 65, 104107.

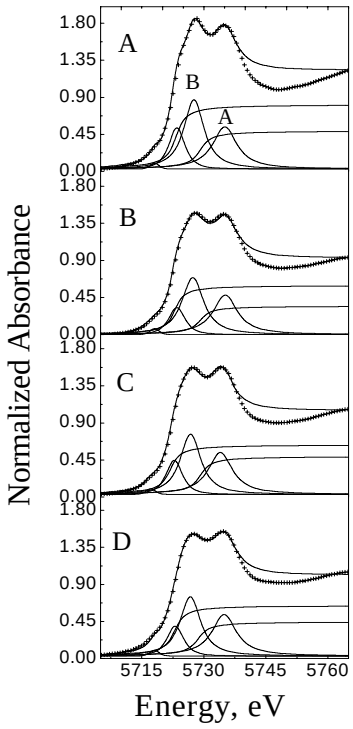

Figure 1. Ce L_{III}-edge XANES spectra with fits of (A) anhydrous CeO_2, (B) hydrous CeO_2, (C) Sample **I**, and (D) Sample **II.**

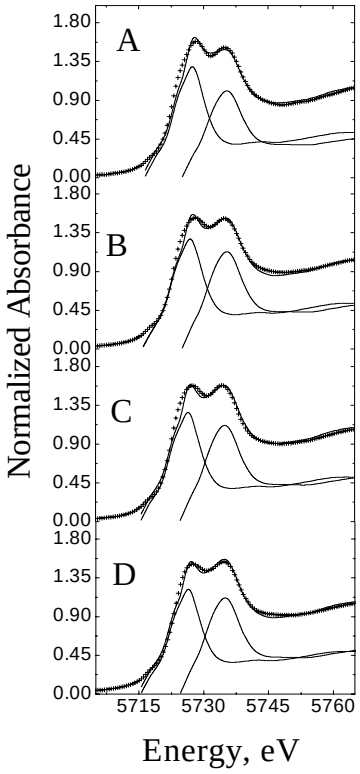

Figure 2. Ce L_{III}-edge XANES spectra with the calculated XANES spectra of (A) anhydrous CeO_2, (B) hydrous CeO_2, (C) Sample **I**, and (D) Sample **II**.

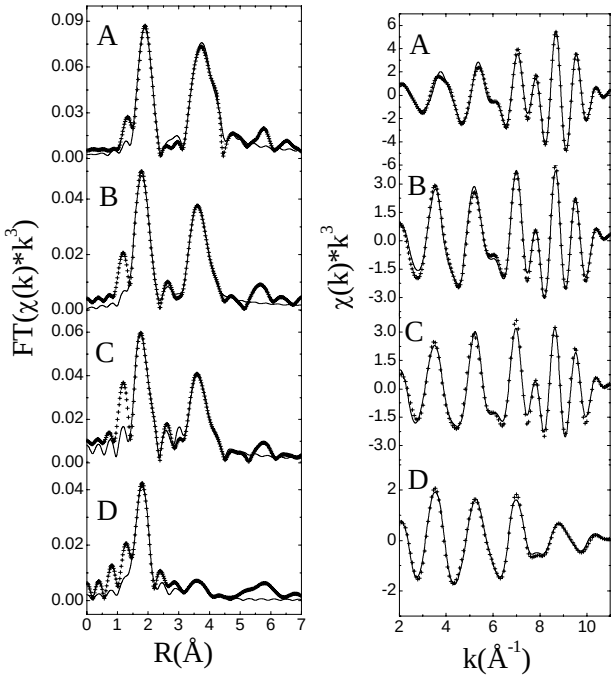

Figure 3. R-space fit result for (A) anhydrous CeO_2, (B) hydrous CeO_2, (C) Sample **I**, and (D) Sample **II**. Right Panel: Corresponding Fourier-filtered data back-transformed fit.